ARTICLE

One-Pot Synthesis of Visible-Light-Driven Plasmonic Photocatalyst Ag/AgCl in Ionic Liquid

Hui Xu, Huaming Li,* Jiexiang Xia, Sheng Yin, Zhijun Luo, Ling Liu, and Li Xu

School of Chemistry and Chemical Engineering, Jiangsu University, Zhenjiang 212013, P. R. China, Jiangsu University Branch Center of State Key Lab of Urban Water Resource and Environment, School of the Environment, Jiangsu University, Zhenjiang 212013, P. R. China

ABSTRACT Plasmonic photocatalyst Ag/AgCl was prepared by in situ hydrothermal method with the contribution of 1-octyl-3-methylimidazolium chloride ([Omim]Cl), in which the [Omim]Cl ionic liquid acted not only as a precursor but also as a reducing reagent in the process of formation of Ag^0. The samples were characterized by X-ray diffraction (XRD), scanning electron microscopy (SEM), diffuse reflectance spectroscopy (DRS), X-ray photoelectron spectroscopy (XPS), and thermogravimetric and differential scanning calorimetry (TG-DSC). The photocatalytic activity of the composites were evaluated by degradation of methyl orange (MO) under visible light irradiation. The experimental results showed that the high activity and stability of Ag/AgCl photocatalysts under visible-light irradiation were due to their localized surface plasmon resonance (LSPR). Based on the characterization of the structure and photocatalytic performance, the LSPR was determined by synergetic effect of many factors, such as particle size of metallic Ag, contents of the Ag^0 nanoparticles, and the extent of metallic Ag dispersing. A photocatalytic mechanism of the Ag/AgCl photocatalyst was also proposed.

KEYWORDS: Plasmonic photocatalyst • Ag/AgCl • Ionic liquid • Localized surface plasmon resonance

1. INTRODUCTION

In recent years, nanostructures of noble metal, especially Ag and Au nanoparticles, have been widely investigated because of their unique features in optical, sensing, and catalysis (1−4). El-Sayed et al. (1) indicate that the interaction of a noble metal nanoparticle with incident light of a specific energy induces intense localized fields at the surface of the noble metal particle. These fields are induced when conduction band electrons of the noble metal nanoparticle couple with the electric field of incident light at a resonant frequency, generating a plasmonic oscillation localized on the surface of the nanoparticle, which was defined as the localized surface plasmon resonance (LSPR) (1). The intrinsic optical and physical properties of Ag and Au nanoparticles are attributed to the LSPR effect (5). The LSPR is strongly affected by many parameters such as morphology, size, and composition of the nanoparticles as well as the dielectric properties of the surrounding medium (1, 6). The noble metal nanoparticles (Ag and Au) have been used as efficient plasmonic photocatalyst because of their LSPR. Awazu et al. (7) have prepared plasmonic photocatalyst TiO_2−Ag/SiO_2. It is found that the photocatalytic activity of TiO_2 can be greatly enhanced if it gets assisted by the near-field amplitudes of localized surface plasmon from the Ag nanoparticles, and the key issue is how to deposit Ag nanoparticles directly onto the silica (SiO_2) shell to prevent oxidation of Ag by direct contact with TiO_2 (7). Chen et al. (8) indicate that Au/ZrO_2 and Au/SiO_2 plasmonic photocatalysts with efficient photocatalytic activity under visible light illumination are due to the LSPR effect of gold nanoparticles. The study in the literature reported that particle size and morphology can affect the LSPR absorption of gold nanoparticles (8).

Recently, Ag/silver halide structures have been used as cocatalysts to enhance photocatalytic activity of semiconductors because of the special property of Ag nanoparticles. Elahifard et al. (9) prepared Ag/AgBr/TiO_2-covered apatite photocatalyst, and the sample had a significantly high photocatalytic activity for destruction of bacteria under visible light. Zhang et al. (10) prepared visible-light-driven AgBr−Ag−Bi_2WO_6 nanojunction by a facile deposition−precipitation method, and the sample shows higher activity for the Procion Red MX-5B degradation. Hu et al. (11) also demonstrated that the introduction of Ag/AgBr in TiO_2 can enhance the photocatalytic activity. The results indicate that Ag/AgBr is the main photoactive species for the destruction of azodyes and bacteria under visible light (11). Tada and coworkers report that Ag@AgCl-loaded α-Fe_2O_3 film photocatalysts prepared by a two-step electrochemical method exhibit high visible light-driven reactivity (12). The microcomposite Ag@AgCl crystal-loaded TiO_2 has been also prepared by a two-step electrochemical method, showing that Ag@AgCl/TiO_2/SnO_2 catalyst exhibits higher photoreactivity than TiO_2/SnO_2 and Ag/TiO_2/SnO_2 (13). These findings are attributable to the function of Ag@AgCl composites as an excellent charge-separation promoter and built-in acceptor (12, 13). Yu et al. (14) introduced the Ag/AgCl

* Corresponding author. Tel.: +86-511-88791800. Fax: +86-511-88791708. E-mail: lihm@ujs.edu.cn.

Received for review August 23, 2010 and accepted December 6, 2010

DOI: 10.1021/am100781n

Published on Web 12/28/2010

structure into TiO_2 nanotube arrays, and indicate that the Ag/AgCl/TiO_2 nanotube array plasmonic photocatalyst shows high visible-light photocatalytic activity and stability during photocatalytic degradation of methyl orange in water. All the above discussion indicates that the Ag/silver halide species (Ag/AgCl or Ag/AgBr structure) can efficiently enhance the photocatalytic activity of the samples.

In a few years, it is also interesting to know the photocatalytic activity of the pure Ag/AgCl or Ag/AgBr structure. Huang et al. (15) synthesized the Ag@AgBr photocatalyst by a two-step method, which is efficient for MO degradation under visible-light illumination. Huang et al. (16) also prepared Ag@AgCl plasmonic photocatalyst. The Ag@AgCl photocatalyst was prepared by mixing Ag_2MoO_4 with HCl to form AgCl powder and then reducing some Ag^+ ions in the surface region of the AgCl particles to Ag^0 under visible-light irradiation (16). It is found that the silver nanoparticles directly deposit on the surface of AgCl particles, and the sample is highly efficient and stable under visible-light illumination (16). Therefore, Ag/silver halide structures are efficient visible-light photocatalyst, and it is also demonstrated that the high photocatalytic activity of the Ag/silver halide catalysts is due to the LSPR of the Ag nanoparticles. However, the synthesis method is complex. The multiple-step approach and the use of UV irradiation are time-consuming and size of the Ag particles on the AgCl surface is not yet well controlled.

In many works, ionic liquids only acted as solvents or templates (17, 18). Few literature reports used ionic liquids as reaction source, and few works focused on their reducing property. Therefore, in this work, the experiment designed a one-pot, novel, simple, and clean approach to prepare the Ag/AgCl plasmonic photocatalyst. The ionic liquid 1-octyl-3- methylimidazolium chloride ([Omim]Cl) was introduced to the synthesis system, in which the room-temperature ionic liquid served not only as the Cl source but also as a reducing reagent of Ag^0 during the one-pot hydrothermal synthesis.

In this work, the photocatalytic activity of the composites was evaluated by the degradation of methyl orange (MO) under visible light irradiation. The influence of particle size of metallic Ag, contents of the Ag^0 nanoparticles and the extent of metallic Ag dispersing on the LSPR of Ag nanoparticles was discussed on the basis of systematic characterization analysis, such as XRD, XPS, SEM-EDS, and DRS. The photocatalytic mechanism of the Ag/AgCl photocatalyst was also proposed.

2. EXPERIMENTAL SECTION

2.1. Material. All chemicals were analytical grade and used as received without purification. The ionic liquid 1-octyl-3-methylimidazolium chloride ([Omim]Cl) (99%) was purchased from Shanghai Chengjie Chemical Co. LTD.

2.2. Preparation of Photocatalysts. The Ag/AgCl composites were synthesized through a simple hydrothermal method with the contribution of [Omim]Cl ionic liquid. In a typical procedure, a certain $AgNO_3$ solution was added dropwise into [Omim]Cl solution. The white precipitates formed immediately. The solution was stirred for 20 min in an open system. Then the mixture was transferred into a Teflon-lined stainless steel autoclave with 30 mL of capacity. The sealed tank was put into an oven and heated at 120 °C for 24 h. The final products were collected by centrifugation, washed with deionized water and ethanol for several times, and then dried at 60 °C for 8 h. The molar ratios of $AgNO_3$/[Omim]Cl (R) were set as 4:1, 3:1, 2:1, and 1:1 respectively. The samples (in the condition of $R = 1{:}1$) heated at 60, 80, 100, 120, 140, and 160 °C for 24 h were respectively named T60, T80, T100, T120, T140, and T160.

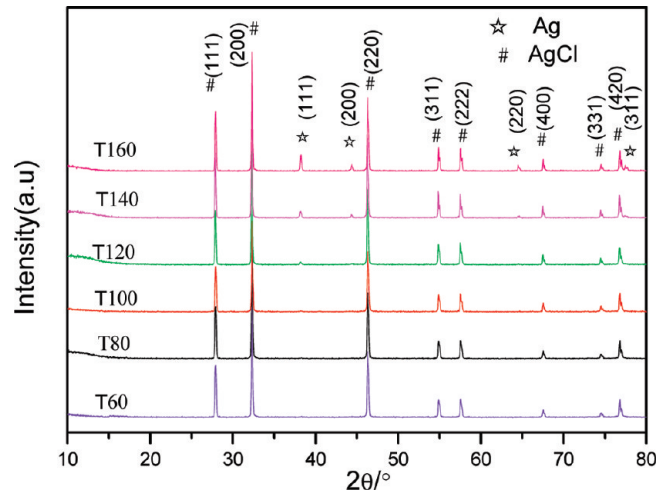

FIGURE 1. XRD patterns of Ag/AgCl synthesized by the hydrothermal process at different temperature. All the samples were prepared with $R = 1{:}1$ for 24 h.

2.3. Characterization of Photocatalysts. The crystalline phases of Ag/AgCl composites were analyzed by X-ray diffraction (XRD) by Bruker D8 diffractometer with Cu$K\alpha$ radiation (λ = 1.54 Å) in the range of $2\theta = 10-80°$. The morphology and particle size of Ag/AgCl powders were obtained by JEOL JSM-7001F field-emission microscope. The chemical composition of the samples was determined by X-ray energy dispersion spectrum (EDS). The diffuse reflectance spectra (DRS) were measured by a UV−vis spectrometer (UV-2450, Shimadzu) in the range of 240 to 800 nm. $BaSO_4$ was used as the reflectance standard material. X-ray photoelectron spectroscopy (XPS) analysis were performed on an VG MiltiLab 2000 X-ray photoelectron spectrometer using the Mg $K\alpha$(1253.6 eV) radiation. Thermogravimetric and differential scanning calorimetry (TG-DSC) analysis were done on STA-449C Jupiter (NETZSCH Corporation, Germany).

2.4. Photocatalytic Activity. Photocatalytic activity of the composites was evaluated by the degradation of MO under visible-light irradiation. Experiments were carried out in Pyrex photocatalytic reactor with two 150 W tungsten halogen lamps as visible light source(λ >400 nm). The distance between the light source and the Pyrex glass was about 20 cm. 0.1 g of photocatalyst was added into 100 mL of MO dye solution (10 mg L^{-1}). Prior to irradiation, the solution was stirred magnetically in the dark for 30 min in order to reach the adsorption-desorption equilibrium between the photocatalyst and the MO dye. The concentration of the MO solution was monitored using a UV−vis spectrophotometer. The absorbance of MO was determined by spectrophotometer at 464 nm.

3. RESULTS AND DISCUSSIONS

3.1. XRD Analysis. The XRD patterns for Ag/AgCl composites with different hydrothermal conditions were shown in Figure 1. All patterns matched very well with the JPCDS standard data of AgCl (JCPDS file: 31-1238). The peaks at $2\theta = 27.82$, 32.24, 46.25, 54.81, 57.56, 67.4, 74.5, and 76.6° were assigned to the (111), (200), (220), (311), (222),

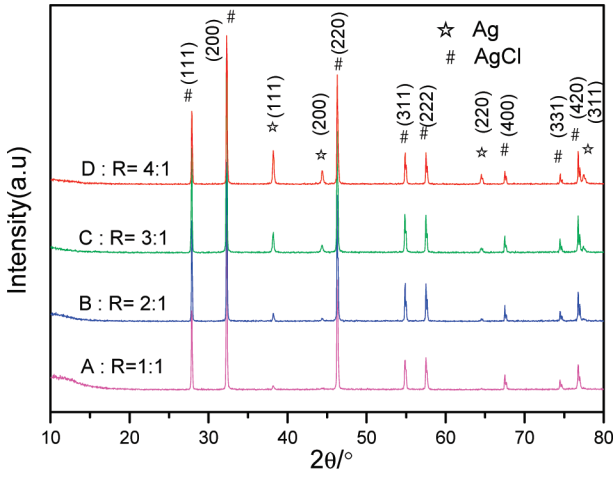

FIGURE 2. XRD patterns of the Ag/AgCl samples prepared with various *R* values at 120°C for 24 h. *R* = (A) 1:1, (B) 2:1, (C) 3:1, (D) 4:1.

(400), (331), and (420) planes of cubic phase of AgCl crystal, which were marked with "#". With the increasing hydrothermal temperature of as-prepared products, the diffraction peaks at 38.1, 44.3, 64.2 and 77.5° gradually appeared and the intensity increased with the increase of hydrothermal temperature. The four diffraction peaks were respectively matched with the (111), (200), (220), and (311) crystalline planes of metallic Ag, which marked with "☆". The positions of the four peaks could be well-indexed to cubic phase Ag (metallic Ag, JCPDS file: 65-2871). No other peaks of impurities or other phases such as Ag_xO were observed in Ag/AgCl composites, indicating that the sample only contained the phase of metallic Ag and AgCl.

Figure 2 showed the XRD patterns of the Ag/AgCl samples with different *R* value (A: 1:1, B: 2:1, C: 3:1, D: 4:1). All the diffraction peaks could be indexed to metallic Ag and AgCl phases. It could be also seen that the intensity of the peaks identified as Ag^0 was gradually increased with the enhancing *R* value, indicating that more metallic Ag formed in the Ag/AgCl composite.

To study the formation mechanism of Ag/AgCl composites, we investigated the influence of the precursor. To confirm the function of the [Omim]Cl ionic liquid, the experiment substituted NaCl for the ionic liquid as the Cl^- source (molar ratio of Ag:Cl = 1:1), and the XRD patterns of the catalysts were shown in Figure S1. The diffraction peaks of the products synthesized under 120°C and 160°C could be indexed to the high crystalline AgCl phase (JCPDS file: 31-1238). However, no characteristic peaks corresponding to metallic Ag were observed. From the comparison between Figure 1 and Figure S1 in the Supporting Information, it could be confirmed that the presence of ionic liquid indeed played a key role in the formation of Ag/AgCl composite. In fact, the ionic liquid acted as a reducing reagent in the process of preparing Ag^0 in the Ag/AgCl structure. The overall chemical reactions could be formulated as follows:

$$AgNO_3 + [Omim]Cl \rightarrow AgCl\downarrow + NO_3^- + [Omim]^+ \quad (1)$$

$$AgCl \xrightarrow[\text{ionic liquid}]{\text{hydrothermal reduce}} Ag^0/AgCl \quad (2)$$

From the chemical structure of [Omim]Cl (see Scheme S1 in the Supporting Information), it could be seen that the $[Omim]^+$ cation in [Omim]Cl had a five-membered heterocyclic ring containing two nitrogen atoms. Zhu et al. (19, 20) believed that the reducing ability of $[Bmim]BF_4$ and poly(vinylpyrrolidone) (PVP) was due to the nitrogen atoms of the five-membered heterocyclic ring. However, it was found that the 2-H in the imidazole ring had different properties (21−23). Arduengo (21) and Tapu (22) indicated that the carbenes could be obtained when the imidazole ring lost 2-H.

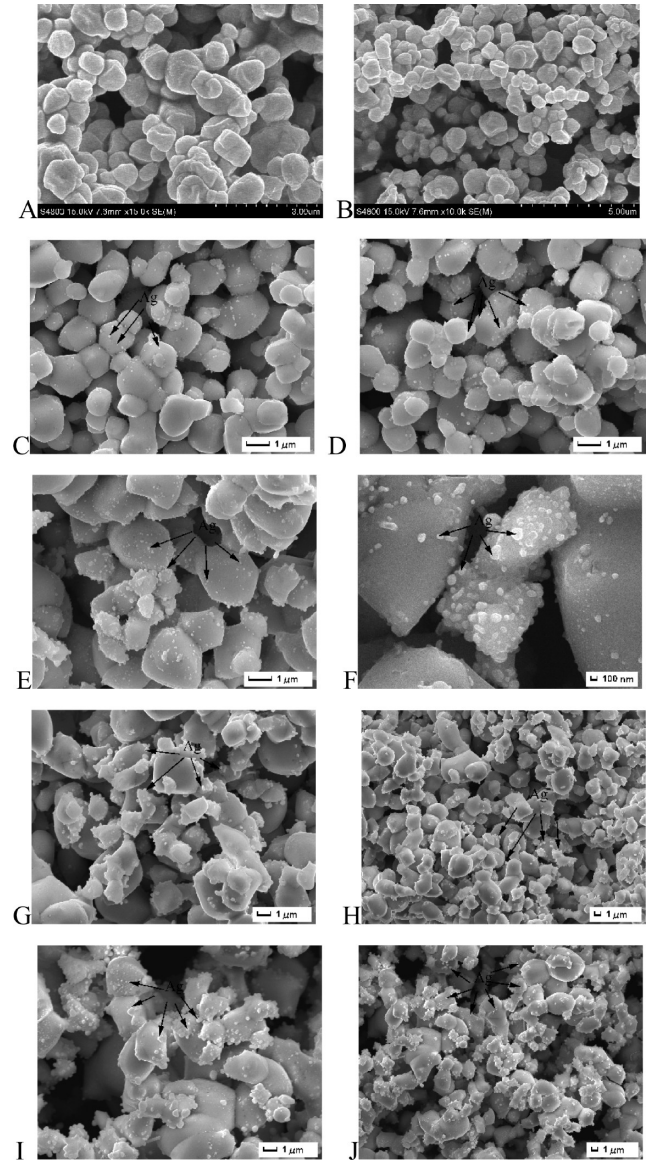

FIGURE 3. SEM micrographs of the products obtained by different hydrothermal temperature: (A, B) T60, (C, D) T80, (E, F) T120, (G, H) T140, (I, J) T160.

Table 1. Estimated Average Diameter of Ag Nanoparticles in Ag/AgCl Composites

catalysts prepared by different hydrothermal temperature	estimated average diameter of Ag nanoparticles in Ag/AgCl composites (nm)
T80	40−80
T120	60−200
T140	200−400
T160	300−700

Sun (23) also reported that the acidic property of the 2-position H of 1-*n*-butyl-3-methylimidazolium chloride ([bmim]Cl) was confirmed by FT-IR and ^{1}H NMR analysis. As for the synthesis of Ag/AgCl photocatalyst in this study, the partial 2-H may escape from the imidazole ring, and the 2-H could change to H^+ (21−23), which finally displayed the Brönsted acidic property. During the above process, the imidazole ring could lose partial 2-H to form carbenes, which had two nonbonding electrons. The partial AgCl might be reduced to Ag^0 due to the electron of the carbenes. So the formed carbenes possibly played a role in reducing Ag^+. Therefore, we deduced that the reducing property might be due to the electron of the carbenes structure.

In conclusion, on the basis of the above analysis, the [Omim]Cl ionic liquid acted not only as a precursor but also as reducing agent to reduce partial Ag^+ of AgCl to metallic Ag.

3.2. SEM-EDS. ***3.2.1. Influence of the Hydrothermal Temperature.*** Figure 3 showed the morphology of Ag/AgCl composites prepared at different hydrothermal temperature. It was found that with increasing hydrothermal temperature, the clear, nice, and tiny particles of Ag nanoparticles were covering on the surface of the large AgCl. However, there was a little of Ag appearing on the surface of the AgCl at 60°C (Figure 3A, B), indicating that low temperature was not in favor of the Ag^0 reducing. In Figure 3, it could be seen that the size of AgCl did not change, and the estimated average diameter of the AgCl was between 0.3 and 1.5 μm. It was also confirmed that the hydrothermal temperature was an important factor to control the size of Ag^0 nanoparticles in the Ag/AgCl composite. The size of metallic Ag nanoparticles obtained at different hydrothermal temperature was estimated and listed in Table 1. It was observed that particle size of Ag^0 clusters was improved by the increasing temperature. The SEM images indicated that the higher hydrothermal temperature was, the bigger Ag^0 was. When the temperature increased to 80°C, the estimated diameter of Ag nanoparticles was in the range of 40−80 nm (Figure 3C, D). In the condition of hydrothermal temperature at 160°C, the estimated diameter enlarged to 300−700 nm (Figure 3 I and J), and it was noticed that the formed Ag clusters agglomerated together. It could be deduced from the above comparative experiments that the appropriate temperature was important for the preparation of Ag/AgCl structures with special size of Ag nanoparticles.

The composition of the Ag/AgCl structure was also identified by EDS analysis. The EDS image of Ag/AgCl sample prepared at 160°C was shown in Figure S2 in the Supporting Information. The results indicated that the sample was composed of Ag and Cl elements.

3.2.2. The Influence of R Value on the Morphologies of the Samples. The morphology and microproperties of the Ag/AgCl composition with different *R* value were shown in Figure 4. It was found that with the increasing *R* value, the size of metallic Ag developed in Ag/AgCl composition. When $R = 4{:}1$, the presence of ionic liquid accelerated growth and aggregation of Ag^0 nanoparticles. In Figure 4D, it was shown that the surface of the composites consisted of aggregations containing metallic Ag^0 nanoparticles, and the branch morphology of Ag/AgCl was obtained.

3.3. XPS Analysis. To investigate the chemical state of Ag and Cl elements, we carried out XPS measurements. The XPS peaks of Ag 3d and Cl 2p were shown in Figure 5. It was found that the peaks of Ag $3d_{5/2}$ and Ag $3d_{3/2}$ were centered at 367.3 and 373.3 eV, respectively (Figure 5A). The binding energy located at 197.6 eV was consistent with the Cl 2p orbit, illustrating to the existence of Cl^- (Figure 5B). Du et al. (24) indicated that the peaks of metallic silver observed at 368.4 and 374.4 eV could be ascribed to Ag $3d_{3/2}$ and Ag $3d_{5/2}$, respectively. In the case of the Ag/AgCl composites, the peaks ascribed to Ag 3d exhibited the negative shift, which was different from the pure metallic Ag. It might be due to the interaction between Ag nanopar-

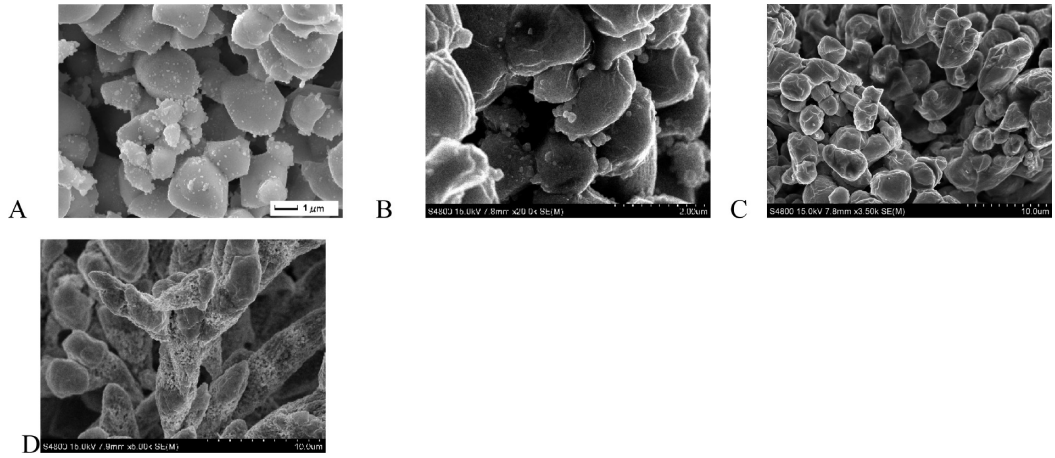

FIGURE 4. SEM images of Ag/AgCl samples with *R* = (A) 1:1, (B) 2:1, (C) 3:1, and (D) 4:1. The hydrothermal temperature was at 120°C for 24 h.

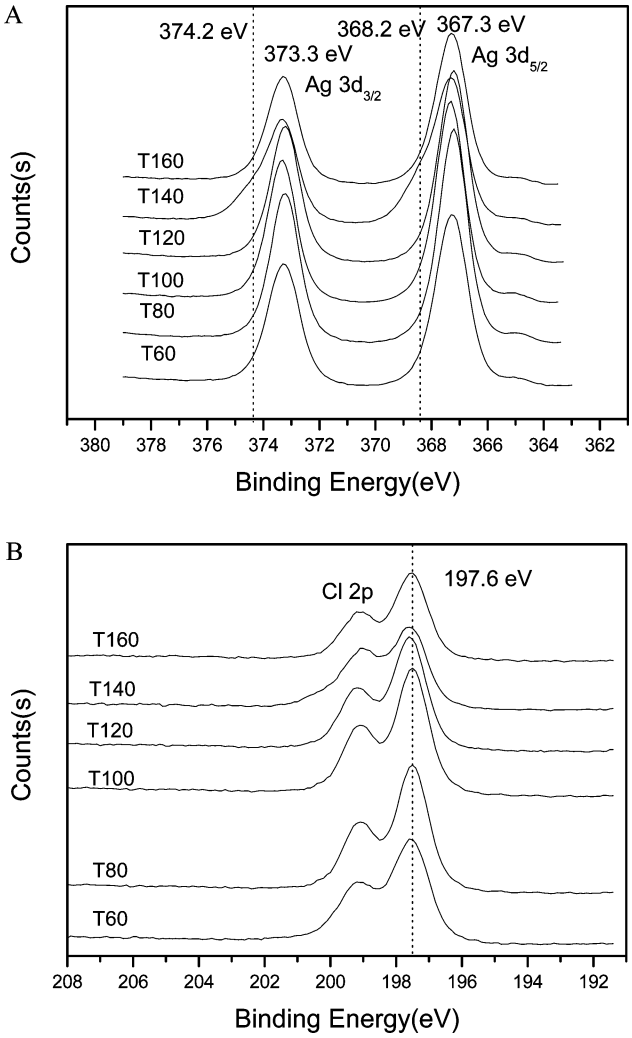

FIGURE 5. Ag 3d (A) and Cl 2p (B) high-resolution XPS spectra of Ag/AgCl samples with different preparing condition.

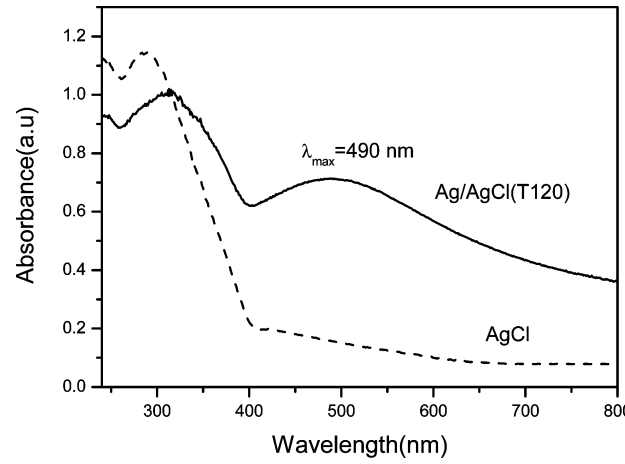

FIGURE 6. DRS spectra of pure AgCl and Ag/AgCl composite (T120, R = 1:1).

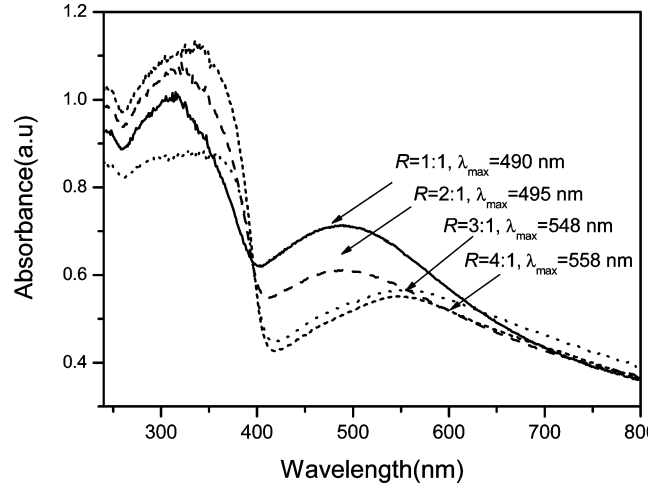

FIGURE 7. DRS spectra of Ag/AgCl composites (T120) with different R values.

ticles and AgCl particles. The above XRD analysis had confirmed that the metallic Ag and AgCl coexisted in the samples. Therefore, the combination of XPS and XRD analysis showed that part of silver in the composites indeed existed as the metallic state. Surface Ag^0 contents were calculated by XPS data, and the value of Ag^0/Ag^+ was shown in Table S1 in the Supporting Information. It was noticed that the contents of Ag^0 improved with the increase of hydrothermal temperature and R value, which was well-consistent with the XRD analysis.

3.4. DRS. The DRS spectra of the pure AgCl and Ag/AgCl (T120, R=1:1) were shown in Figure 6. It was found that the absorption band of the pure AgCl was in the region of 240−400 nm. In the case of the Ag/AgCl composite, two prominent absorption bands were observed in UV-visible region. The former could be attributed to the absorption of the AgCl, and its corresponding absorption edge was located below 400 nm. The latter absorption bands (λ_{max} = 490 nm) could be due to the characteristic absorption of surface plasmon absorption (SPB) of metallic silver covering on the AgCl surface. The SPB was due to the LSPR of metallic Ag nanoparticles (11, 25). The absorption wavelength of the SPB was affected by shape, orientation, and contact area with the substrate (26). The characteristic SPB of pure Ag^0 appeared at about 390 nm (5). Hu et al. (11) indicated that the absorption band of the Ag/TiO_2 catalyst would derive from the surface plasmon absorption of silver at 490−530 nm. A LSP resonance peak could be observed at 410 nm in the case of TiO_2 on the Ag/SiO_2 core−shell structure (7). Therefore, the different surrounding medium could lead to the blue-shift or red-shift of the SPB. The experiment also found that the SPB was related to the particle size of metallic Ag and the composition of the Ag/AgCl catalysts. The optical absorption spectra of Ag/AgCl composites prepared by different R value were shown in Figure 7. The position of the SPB peaks was changed from 495 nm to 558 nm with the enhancing R value. Literature reported that the SPB could be tuned by modulating the composition and/or composition distribution of the compounds (6, 27). In the presence of the Ag/AgCl composites, the change of SPB could be attributed to the bigger metal Ag particles and the increasing Ag^0 content in the samples(Figure 4 and Table S1 in the Supporting Information). In conclusion, the more Ag contents and bigger Ag particle in Ag/AgCl composites led to the larger red shift of the surface plasmon absorption band.

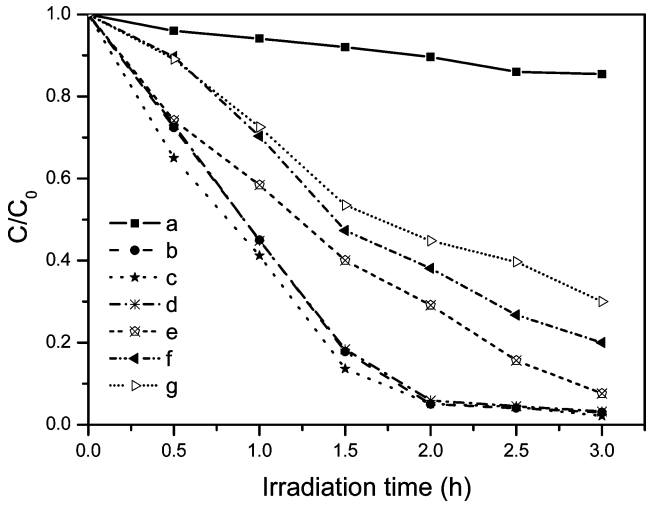

FIGURE 8. Photocatalytic degradation of MO over different Ag/AgCl products prepared with various hydrothermal temperature under visible light irradiation. (a) photolysis without catalysts, (b) T60, (c) T80, (d) T100, (e) T120, (f) T140 and (g) T160.

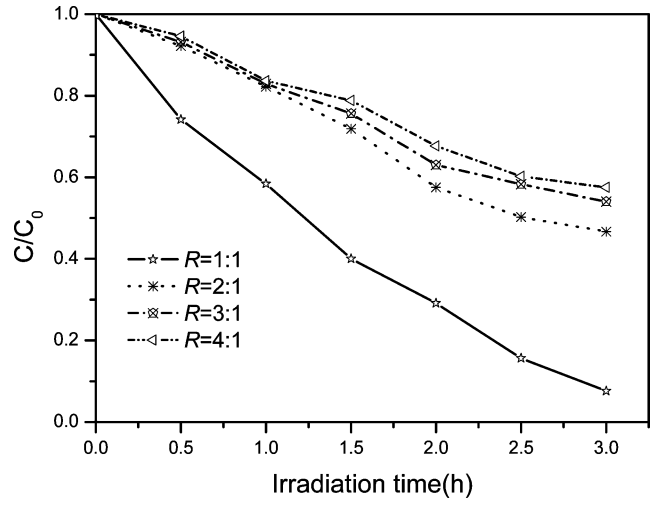

FIGURE 9. Photocatalytic activity of Ag/AgCl samples (T120) obtained with varying *R* for the degradation of MO under visible-light irradiation.

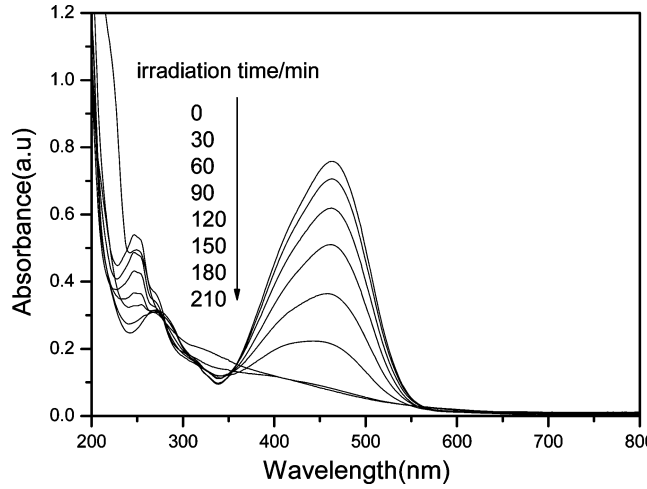

FIGURE 10. Temporal absorption spectral patterns of MO dye during the photodegradation process by Ag/AgCl sample. The preparation condition of the catalyst: *R* = 1:1; hydrothermal temperature,120°C.

The observation from the appearance indicated that the mauve color powder showed there was metallic Ag in the composite. For comparison, the pure AgCl was also prepared. The color of the pure AgCl was white.

3.5. TG-DSC. Figure S3 in the Supporting Information showed the TG-DSC curves of the Ag/AgCl composite. There was no weight loss in the range of 30−800 °C. The results suggested that no significant volatile products were generated. So it was also indicated that the prepared Ag/AgCl photocatalyst was pure. The exothermic peaks at 458.8 °C could be attributed to the decomposition of AgCl during the combustion.

3.6. Photocatalytic Activity of Ag/AgCl Samples. Figure 8 showed the photocatalytic activity of the Ag/AgCl samples prepared at different hydrothermal temperature. The blank test confirmed that 14.6% of MO could be degraded without photocatalysts after 3 h of irradiation. Ag/AgCl obtained at 80 °C exhibited the highest photocatalytic efficiency. 94.9% of MO dye in the solution was removed after 2 h irradiation, indicating that the presence of Ag/AgCl photocatalyst played an important role in the photodegradation of MO. It was found that the photocatalytic activity of the Ag/AgCl composites decreased with the increasing hydrothermal temperature (>80°C). The photocatalytic activity of all the samples was in the following order: T80 > T60 > T100 > T120 > T140 > T160. Figure 9 presented the photodegradation efficiencies of MO in the presence of the photocatalysts prepared by different *R* value (hydrothermal temperature: 120°C). It could be seen that when *R* was 1:1, the photocatalytic degradation efficiency of MO reached 92.3% after 3 h. When *R* value was 2:1, 3:1, and 4:1, the photodegradation efficiencies reached 53.3, 46.0, and 42.5%, respectively. The above results could be related to the LSPR of metallic Ag in the Ag/AgCl composite. Zhang et al. (6) indicated that the factors which could influence LSPR included the size, shape, and composition of the noble nanoparticles. As for the Ag/AgCl structure in this study, the changes of the photocatalyic activity of the samples could be illuminated as follows:

For one thing, in Table 1, it could be found that Ag^0 nanoparticles in the Ag/AgCl samples grew with the enhancing hydrothermal temperature. Generally, the smaller the particle, the higher the photocatalytic activity (28). So the photocatalytic activity of the Ag/AgCl composites decreased with the enhancing hydrothermal temperature. Nevertheless, it was interesting that the photocatalytic activity of the Ag/AgCl sample prepared at 60°C hydrothermal temperature was poorer than that of the sample in the condition of 80°C. In Table S1 in the Supporting Information, it could be seen that the contents of Ag^0 in the composite prepared at 60°C (5.8 wt %) was less than Ag^0 content in T80 (Ag^0 contents: 10 wt %), which means that the intensity of LSPR of T60 was lower than T80, so it led to the decreasing photocatalytic efficiency compared with T80. But when Ag^0 content was higher (>10 wt %, in Table S1 in the Supporting Information), the photocatalytic efficiency of MO was also decreased. Therefore, the content of the metallic Ag nanoparticles was another important factor to affect the LSPR. It

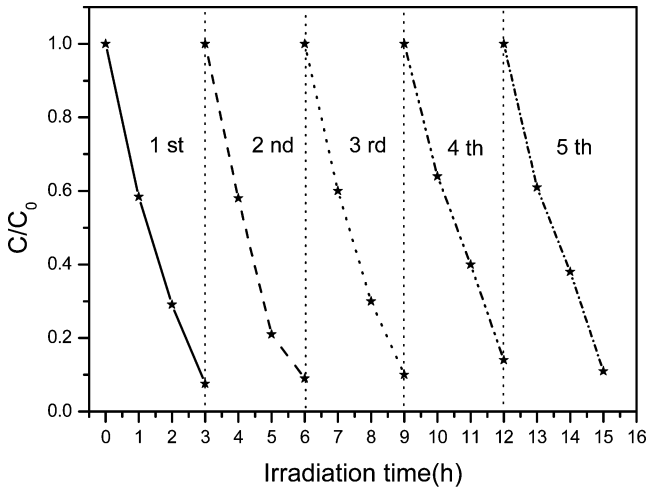

FIGURE 11. Cycling runs in the photocatalytic degradation of MO in the presence of Ag/AgCl (R = 1:1, T120) composite under visible light irradiation.

was very interesting that the photocatalytic activity reduced when the content of Ag^0 was over 10 wt %. It was considered that more Ag^0 on the surface of the AgCl could change the constitutions of Ag/AgCl structure (Figures 3 and 4) and affect the LSPR. It then led to the low photocatalytic activity. In Figures 3 and 4, the morphology and structure of the samples gradually changed to the Ag/AgCl core−shell nanostructures when there was more Ag^0 covering on their surfaces. As a result, the constitution change of Ag/AgCl structure also affected the photocatalytic activity. Ye et al. (29) also indicated that the Ag^0 content could affect the photocatalytic activity of the samples. Therefore, the changes of the structure of the samples could affect the LSPR and photocatalytic activity.

For the other thing, the extent of metallic Ag dispersing also played a key role in enhancing photocatalytic efficiency. It was found that the photodegradation activity of the powders was decreased with the rising R value. From Figure 4, it was noticed that the metallic Ag nanoparticles covering on the surface of AgCl particles generally aggregated together with enhancing R value. When R = 1:1, the Ag clusters well-dispersed on the surface of the catalysts. In Figure 7, the intensity of LSPR of the samples decreased in the following sequence: R = 1:1 > R = 2:1 > R = 3:1 > R = 4:1, which matched with the photocatalytic activity of the composites (Figure 9), which was consistent with previous report (30, 31). Consequently, high dispersing of Ag was beneficial to improve the intensity of LSPR. The content of Ag nanoparticles in the samples prepared by different R value also affected the LSPR, because the content of the Ag^0 in the Ag/AgCl catalysts increased with the increasing R value. Therefore, it could be inferred that the LSPR could be synergetic effect of a number of factors, including particle size of metallic Ag, contents of the Ag^0 nanoparticles and the extent of metallic Ag dispersing, namely, the photocatalytic activity of the Ag/AgCl catalyst was determined by the joint effects of particle size of noble Ag metal, contents of the Ag^0, and the dispersing extent of metallic Ag. So if the LSPR had an optimal value, the photocatalytic activity of the Ag/AgCl sample could have the highest value.

The temporal evolution of the spectral changes taking place during the photocatalytic degradation of MO under visible light irradiation over Ag/AgCl composite was shown in Figure 10. It was found that the MO absorption was decreased rapidly at the wavelength of 464 nm, indicating that the sample exhibited excellent photocatalytic activity. It was also shown that the color of the suspension changed from yellow to colorless, as shown in Figure S4 in the Supporting Information, indicating that the chromophoric structure of the MO dye was destroyed and the MO was almost decomposed.

3.7. Stability of Plasmonic Photocatalyst Ag/AgCl. To confirm the stability of plasmonic photocatalysts Ag/AgCl, we conducted the repeatability experiment of MO degradation, as shown in Figure 11. After five recycles for the photocatalytic degradation of MO solution, the photocatalytic activity of the plasmonic photocatalyst did not decrease significantly under visible light irradiation. The results demonstrated that Ag/AgCl was highly stable photocatalyst under visible light irradiation. Hu et al. (11) reported that silver halides were rather easily decomposed by light illumination to form silver metals. Therefore, it was a very interesting problem why the Ag/AgCl structure had high stability. In the present photocatalytic system, a photon from the visible light irradiation could be absorbed by the metallic silver nanoparticles because of the LSPR, and the absorbed photon would be efficiently decomposed into an electron and a hole (14−16). The LSPR could result in enhancement

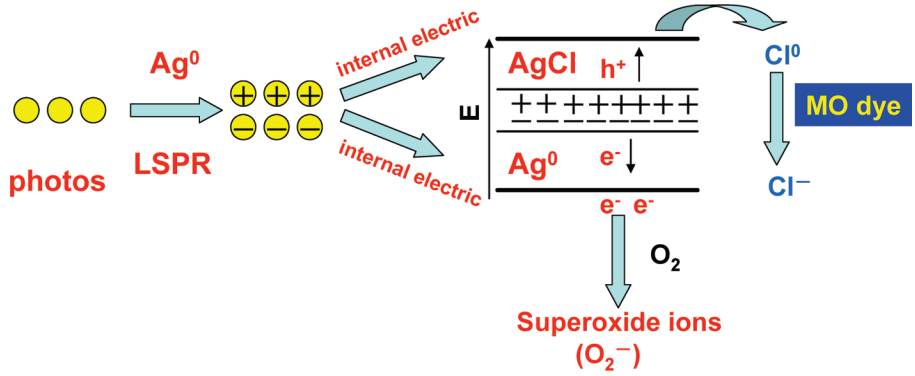

FIGURE 12. Schematic model of the photocatalytic mechanism for Ag/AgCl composite.

of the local inner electromagnetic field (16). The generated electron and hole could be separated efficiently with the help of the local electromagnetic field. Due to the local electromagnetic field, the electron remained in the nanoparticles but not being transferred to the Ag^+ ions of the AgCl lattice. The photogenerated electron could be transferred to the present molecular oxygen to form the active species (14). The active species would then degrade the MO dye. Nevertheless, the left hole was transferred to the AgCl surface due to the negative charge (14), which could cause the oxidation of Cl^- ions to Cl^0 atoms (15, 16). It was consistent with Huang and Yu's reports (15, 16). Because of the high oxidation ability of the chlorine atoms, the MO dye could be oxidized by the chlorine atoms and hence the Cl^0 could be reduced to chloride ions again (16). So the Ag/AgCl composite could remain stable without deterioration. In conclusion, the LSPR of metallic silver played a key role in enhancing the stability of the photocatalyst. The change of LSPR affected the local electromagnetic field, which could influence the separation rate of the photogenerated electron and hole, and finally affect the photocatalytic activity of the composites. On the basis of the above observations, the photocatalytic mechanism of plasmonic photocatalyst Ag/AgCl was proposed in Figure 12.

4. CONCLUSIONS

To sum up, the visible-light-activity plasmonic photocatalyst Ag/AgCl had been successfully synthesized through a facile one-pot hydrothermal method in [Omim]Cl ionic liquid. The [Omim]Cl played not only as a Cl source but also as the reducing reagent of Ag^0. The Ag/AgCl composite was efficient and stable for MO degradation under visible light irradiation. The LSPR of metallic Ag nanoparticle could be influenced by the synergetic effect of many factors, which consisted of particle size of metallic Ag, contents of the Ag^0 nanoparticles, and the extent of metallic Ag dispersing. As a result, the change of LSPR could lead to the different photocatalytic activity of the composites.

Acknowledgment. The authors genuinely appreciate the financial support of this work from the National Nature Science Foundation of China (21007021, 21076099 and 20876071), Research Foundation of Jiangsu University (10JDG128), and the Doctoral Innovation Fund of Jiangsu (CX09B-210Z).

Supporting Information Available: Information on the characterization of AgCl and Ag/AgCl catalysts by XRD, EDS, XPS, and TG-DSC. This material is available free of charge via the Internet at http://pubs.acs.org.

REFERENCES AND NOTES

(1) Tabor, C.; Murali, R.; Mahmoud, M.; El-Sayed, M. A. *J. Phys. Chem. A* **2009**, *113*, 1946–1953.
(2) Crooks, R. M.; Zhao, M. Q.; Sun, L.; Chechik, V.; Yeung, L. K. *Acc. Chem. Res.* **2001**, *34*, 181–190.
(3) Huang, W.; Qian, W.; El-Sayed, M. A. *Adv. Mater.* **2008**, *20*, 733–737.
(4) Rosi, N. L.; Mirkin, C. A. *Chem. Rev.* **2005**, *105*, 1547–1562.
(5) Liang, H.; Yang, H.; Wang, W.; Li, J.; Xu, H. *J. Am. Chem. Soc.* **2009**, *131*, 6068–6069.
(6) Zhang, Q.; Tan, Y. N.; Xie, J.; Lee, J. Y. *Plasmonics* **2009**, *4*, 9–22.
(7) Awazu, K.; Fujimaki, M.; Rockstuhl, C.; Tominaga, J.; Murakami, H.; Ohki, Y.; Yoshida, N.; Watanabe, T. *J. Am. Chem. Soc.* **2008**, *130*, 1676–1680.
(8) Chen, X.; Zhu, H. Y.; Zhao, J. C.; Zheng, Z. F.; Gao, X. P. *Angew. Chem. Int. Ed.* **2008**, *47*, 5353–5356.
(9) Elahifard, M. R.; Rahimnejad, S.; Haghighi, S.; Gholami, M. R. *J. Am. Chem. Soc.* **2007**, *129*, 9552–9553.
(10) Zhang, L.; Wong, K. H.; Chen, Z.; Yu, J. C.; Zhao, J.; Hu, C.; Chan, C. Y.; Wong, P. K. *Appl. Catal. A* **2009**, *363*, 221–229.
(11) Hu, C.; Lan, Y.; Qu, J.; Hu, X.; Wang, A. *J. Phys. Chem. B* **2006**, *110*, 4066–4072.
(12) Nakajima, Y.; Jin, Q.; Tada, H. *Electrochem. Commun.* **2008**, *10*, 1132–1135.
(13) Morimoto, T.; Suzuki, K.; Torikoshi, M.; Kawahara, T.; Tada, H. *Chem. Commun.* **2007**, 4291–4293.
(14) Yu, J.; Dai, G.; Huang, B. *J. Phys. Chem. C* **2009**, *113*, 16394–16401.
(15) Wang, P.; Huang, B.; Zhang, X.; Qin, X.; Jin, H.; Dai, Y.; Wang, Z.; Wei, J.; Zhan, J.; Wang, S.; Wang, J.; Whangbo, M. H. *Chem. Eur. J.* **2009**, *15*, 1821–1824.
(16) Wang, P.; Huang, B.; Qin, X.; Zhang, X.; Dai, Y.; Wei, J.; Whangbo, M. H. *Angew. Chem. Int. Ed.* **2008**, *47*, 7931–7933.
(17) Dahl, J. A.; Maddux, B. L. S.; Hutchison, J. E. *Chem. Rev.* **2007**, *107*, 2228–2269.
(18) Welton, T. *Chem. Rev.* **1999**, *99*, 2071–2084.
(19) Yang, L. X.; Zhu, Y. J.; Wang, W. W.; Tong, H.; Ruan, M. L. *J. Phys. Chem. B* **2006**, *110*, 6609–6614.
(20) Zhu, Y. J.; Hu, X. L.; Wang, W. W. *Nanotechnology* **2006**, *17*, 645–650.
(21) Arduengo, A. J. III.; Dias, H. V. R.; Harlow, R. L.; Kline, M. *J. Am. Chem. Soc.* **1992**, *114*, 5530–5534.
(22) Tapu, D.; Dixon, D. A.; Roe, C. *Chem. Rev.* **2009**, *109*, 3385–3407.
(23) Sun, X.; Zhao, S.; Wang, R. *Chin. J. Catal.* **2004**, *25*, 247–251.
(24) Du, J.; Zhang, J.; Liu, Z.; Han, B.; Jiang, T.; Huang, Y. *Langmuir* **2006**, *22*, 1307–1312.
(25) Zheng, Y.; Zheng, L.; Zhan, Y.; Lin, X.; Zheng, Q.; Wei, K. I. *Inorg. Chem.* **2007**, *46*, 6980–6986.
(26) Tanabe, I.; Matsubara, K.; Standridge, S. D.; Kazuma, E.; Kelly, K. L.; Sakai, N.; Tatsuma, T. *Chem. Commun.* **2009**, 3621–3623.
(27) Yoon, J. W.; Sasaki, T.; Koshizaki, N. *Thin Solid Films* **2005**, *483*, 276–282.
(28) Arabatzis, I. M.; Stergiopoulos, T.; Andreeva, D.; Kitova, S.; Neophytides, S. G.; Falaras, P. *J. Catal.* **2003**, *220*, 127–135.
(29) Bi, Y.; Ye, J. *Chem. Commun.* **2009**, 6551–6553.
(30) Zheng, Y.; Chen, C.; Zhan, Y.; Lin, X.; Zheng, Q.; Wei, K.; Zhu, J. *J. Phys. Chem. C* **2008**, *112*, 10773–10777.
(31) Zhang, H.; Chen, G. *Environ. Sci. Technol.* **2009**, *43*, 2905–2910.

AM100781N